Biochemical and Biophysical Research Communications 438 (2013) 457–461

Contents lists available at ScienceDirect

Biochemical and Biophysical Research Communications

journal homepage: www.elsevier.com/locate/ybbrc

Crystal structures of 26 kDa *Clonorchis sinensis* glutathione S-transferase reveal zinc binding and putative metal binding

Young-Hyun Han [a,b], Sung-Jong Hong [c], Hae-Kap Cheong [a,*], Yong Je Chung [b,*]

[a] Division of Magnetic Resonance Research, Korea Basic Science Institute (KBSI), Ochang, Chungbuk 363-883, Republic of Korea
[b] Department of Biochemistry, Chungbuk National University, Cheongju 361-763, Republic of Korea
[c] Department of Medical Environmental Biology, College of Medicine, Chung-Ang University, Dongjak-gu, Seoul 156-756, Republic of Korea

ARTICLE INFO

Article history:
Received 19 July 2013
Available online 31 July 2013

Keywords:
*Cs*GST
*Cs*GST–D26H mutant
Zinc coordination
Crystal structure
Crystal packing

ABSTRACT

The crystal structures of *Cs*GST in two different space groups revealed that Asp26 and His79 coordinate a zinc ion. In one space group, His46 of an adjacent molecule participates in the coordination within 2.0 Å. In the other space group, Asp26, His79 and a water molecule coordinate a zinc ion. The *Cs*GST–D26H structure showed that four histidine residues – His26 and His79 from one molecule and the same residues from a symmetry-related neighboring molecule – coordinate a zinc ion. The coordinated zinc ions are located between two molecules and mediate molecular contacts within the crystal.

1. Introduction

Glutathione S-transferases (GSTs) are well-known enzymes that play a key role in enzymatic detoxification. They catalyze the nucleophilic addition of the thiol group of glutathione to a wide variety of electrophilic endo- and xeno-substrates [1,2]. The glutathione-conjugated substrates are more water-soluble and can be easily discharged from cells. GSTs are ubiquitously found in wide range of bio-organisms from mammals to bacteria. Based on their cellular localization, GSTs can be divided into the following three subgroups: mitochondrial, microsomal, and cytosolic [3]. Cytosolic GSTs are classified into several classes on the basis of substrate specificity, sequence and structural similarity as follows: alpha, mu, pi, kappa, omega, and theta classes in mammals and sigma, zeta, beta classes, fungi, plants, insects, and helminths in non-mammals [4]. The structural and functional characteristics of a number of GSTs have been well studied. The three-dimensional structures of GSTs have been determined and revealed that GSTs exist as homo or hetero-dimers, and each monomer of GSTs is composed of two domains, a smaller N-terminal α/β domain and a larger C-terminal α-domain [1,5,6]. The N-terminal domain, in which GSH is bound, adopts a thioredoxin-like fold that consists of four β-strands and three α-helices. The C-terminal domain shares all α-helices and serves as the binding site for a range of substrates [5,6]. Although GSTs share this common folding pattern, the structures of each class have characteristic features, particularly concerning the substrate-binding site.

The crystal structures of some GSTs have been determined from the helminths *Schistosoma japonicum* (*Sj*GST), *Fasciola hepatica* (*Fh*GST) and *Necator americanus* (Na-GST) [7–11]. The *Sj*GST and the *Fh*GST are classified as mu class, but they lack the mu loop between the β2 strand and α2 helix that is characteristic of mammalian mu class structures. Enzymatic detoxification has been classified into three distinct phases in mammals. The cytochrome P-450 system is primarily responsible for phase I and turns xenobiotics into epoxide-containing compounds. GSTs play a major role in phase II detoxification by catalyzing the conjugation of endogenous GSH to the xenobiotics activated by phase I [4]. In helminths, because cytochrome P-450-dependent detoxification is absent, GSTs carry out most of the detoxification process [12–14]. Detoxifying enzymes have been considered as potential chemo- and immuno-therapeutic targets [15,16]. Inhibitors of *Sj*GST have been developed as anti-parasite agents [17].

*Sj*GST is widely used as a fusion partner in mammalian and bacterial expression systems [18]. It is reported that the human GST M1-1 and A1-1 isozymes have been altered to induce nickel-binding affinity by introducing adjacent histidine residues, and a glutamate to histidine mutation of *Sj*GST resulted in increased nickel-binding affinity [19–21].

In this study, we determined the crystal structures of *Clonorchis sinensis* 26 kDa GST (*Cs*GST) in complex with GSH. The structures are very similar to that of *Sj*GST and harbor a zinc ion in one mono-

* Corresponding authors. Fax: +82 43 267 2306.
E-mail addresses: haekap@kbsi.re.kr (H.-K. Cheong), chungyj@chungbuk.ac.kr (Y.J. Chung).

0006-291X/$ - see front matter © 2013 Elsevier Inc. All rights reserved.
http://dx.doi.org/10.1016/j.bbrc.2013.07.102

mer. Mutation of Asp26 to histidine alters zinc ion coordination and crystal packing. The substituted histidines participate in zinc coordination.

2. Material and methods

2.1. Cloning and site-directed mutagenesis

The coding gene for *Cs*GST was amplified by PCR using the forward primer 5′-GTCGAATTCCATGGCTCCCGTATTGGGCTAC-3′ and the reverse primer 5′-AACTCG AGGTTATTTCGGAGGAGCATCGC-CAC-3′ from the template described previously [23,22]. The PCR products were ligated into pET25b plasmids from which the pelB leader sequence had been removed and that were treated with the endonuclease *BamHI* and *XhoI*.

In order to mutate *Cs*GST Asp26 to His, the above construct was modified by site-directed mutagenesis with the forward primer 5′-CTGGAGTACGTCGGTCATAGTTACGAAGAAC AT-3′ and the reverse primer 5′-ATGTTCTTCGTAACTATGACCGACGTACTCCAG-3′ using the QuikChange site-directed mutagenesis kit (Stratagene) following the manufacturer's instructions.

2.2. Protein expression and purification

The *Escherichia coli* BL21(DE3) expression strain was transformed by the plasmids harboring recombinant *Cs*GST and the *Cs*GST–D26H mutant gene and cultured at 37 °C in LB media. Production of the recombinant protein was induced by adding isopropyl β-D-1-thiogalactopyranoside (IPTG) to the culture medium at an A_{600} of 0.7 to a final concentration of 1 mM, and the cultures were held at 20 °C overnight. After harvesting by centrifugation, the cells were resuspended in 20 mM potassium phosphate buffer pH 7.0 and 5 mM EDTA and lysed by sonication. The supernatants were loaded onto a GSH affinity column and eluted with 15 mM GSH [22]. The eluted *Cs*GST and *Cs*GST–D26H mutant were applied to a Superdex 75 16/60 gel-filtration column (GE Healthcare) pre-equilibrated with 20 mM potassium phosphate buffer pH 7.0 and 100 mM NaCl. Fractions containing the *Cs*GST and *Cs*GST–D26H mutant were concentrated to 14 mg/ml for crystallization.

2.3. Crystallization, data collection and structure determination

One native crystal was obtained in the described method [22]. The other crystals and the *Cs*GST–D26H crystals were grown in 0.1 M Tris pH 8.5 solution containing 5 mM zinc sulfate and 2.0 M ammonium sulfate. These crystals were soaked in cryoprotectant solution containing glycerol at a final concentration of 18% (v/v) and flash cooled in the nitrogen stream at 100 K. X-ray diffraction data of *Cs*GST and *Cs*GST–D26H were collected using the ADSC Quantum 315r and Quantum210 CCD detector with synchrotron radiation at Pohang Accelerator Laboratory (PAL) beamline 4A and beamline 6C (Pohang, Korea). All data sets were integrated and scaled using HKL2000 [23] and iMosflm [24]. The structure of *Cs*GST was calculated by molecular replacement using MOLREP [25] and *Sj*GST (PDB ID: 1M9A) as the search model. The initial model was built with COOT [26] and refined with REFMAC5 [27]. A strong peak in the electron density was determined to be a zinc ion based on the metal ion geometry.

X-ray data collection and refinement statistics are provided in Table 1. The coordinates of two structures of *Cs*GST and the *Cs*GST–D26H mutant have been deposited in the RCSB Protein Data Bank with accession codes 3ISO, 4L5L and 4L5O, respectively.

3. Results

3.1. Structural features

*Cs*GST crystals were obtained from solutions containing 0.1 M MES pH 6.5, 5 mM zinc sulfate, and 10% PEG MME 550 and 0.1 M Tris pH 8.5, 5 mM zinc sulfate, and 2.0 M ammonium sulfate. The

Table 1
Data collection and refinement statistics.

	Native 1	Native 2	D26H
	Data collection		
Space group	$P2_12_12_1$	$P3_221$	$P3_121$
Unit cell parameters			
a, *b*, *c* (Å)	66.27, 67.45, 120.70	96.39, 96.39, 115.42	98.37, 98.37, 178.50
α, β, γ (°)	90, 90, 90	90, 90, 120	90, 90, 120
Wavelength	1.23985	1.00000	1.00000
Resolution (Å)	50.0–2.2	50.0–1.9	59.5–2.09
R_{merge}	0.052 (0.172)[a]	0.058 (0.130)	0.193 (1.928)
Completeness (%)	99.0 (98.5)	99.9 (100)	100 (99.9)
Redundancy	5.4 (4.4)	10.5 (10.2)	5.9 (5.7)
No. of unique reflections	28,185	49,367	60,028
$I/\sigma(I)$	19.2	20.0	7.2
	Refinement		
Resolution (Å)	50.0–2.2	50.0–1.9	50.5–2.09
R_{work}/R_{free}	0.188/0.253	0.179/0.226	0.201/0.249
No. of atoms			
Protein	3524	3540	5296
Ligand	40	40	60
Ion	26	42	32
Water	187	253	255
B-factors			
Protein	26.66 (A), 38.46 (B)	18.61 (A), 16.71 (B)	41.00 (A), 41.88 (B), 35.41 (C)
Ligand	36.89	19.50	44.15
Ion	41.05 (Zn)	22.77 (Zn)	53.19 (Zn)
	51.33 (MES)	46.14 (SO_4)	63.73 (SO_4)
Water	36.157	24.71	40.19
R.M.S. deviations			
Bonds (Å)	0.021	0.030	0.016
Bond angles (°)	2.019	2.187	1.771

[a] Values in parentheses refer to the highest-resolution shell.

crystals grown in MES pH 6.5 belong to the orthorhombic space group $P2_12_12_1$ with unit cell parameters $a = 66.272$, $b = 67.455$, $c = 120.701$ Å, $\alpha = \beta = \gamma = 90°$. One dimer occupied the non-crystallographic asymmetric unit. The crystals obtained in the Tris pH 8.5 solution belonged to the trigonal $P3_221$ space group with unit cell parameters $a = b = 96.390$, $c = 115.428$ Å, $\gamma = 120°$. A non-crystallographic threefold axis generates one dimer per asymmetric unit. The structures of *Cs*GST from different crystal systems were solved by molecular replacement (MR) using the program MOLREP [25] with *Sj*GST (PDB ID: 1M9A) as the search model. The models were refined in REFMAC5 [27] to an *R*-factor 18.8%, *R*-free 25.3% at 2.2 Å in the orthorhombic crystal system, and an *R*-factor 17.9% and *R*-free 22.6% at 1.9 Å in the trigonal crystal system (Table 1).

The *Cs*GST structures share high structural similarity to *Sj*GST. Each monomer of *Cs*GST consists of two domains, the N-terminal G-domain (1–79) and the C-terminal H-domain (86–217) connected by a short linker. The G-domain adopts an α/β fold in which the βαβ and ββα motifs are linked by an α-helix. The G-domain shows high structural conservation in the glutathione (GSH) binding domain. The H-domain contains six helices (86–195) and a long loop tail (Fig. 1A).

The G-domain of each monomer contacts the H-domain of the other monomer to form the dimerization interface. Met94, Ile95, Met132, Trp133 and Phe136 of the H-domain of one monomer are clustered and make a concave hydrophobic pocket where the protruding Leu52 of the other monomer forms a hydrophobic interaction in a knob-and-hole manner (Fig. 1B).

A structural characteristic of GSTs is a *cis*-proline residue located in the N-terminal domain that participates in the interaction with glutathione, γGlu–Cys–Gly. The *cis*-proline is conserved in the G-domain of GST, which has a thioredoxin-like fold and contributes to conformation stability, substrate recognition, and catalytic function [5,28]. *Cs*GST has two *cis*-proline residues, Pro56 and Pro202. The *cis*-conformation of Pro202 in the C-terminal long loop region is characteristic of helminth GSTs. The *cis*-Pro56 interacts with the γ-glutamyl moiety of GSH through a water-mediated hydrogen bond. The adjacent two residues, Asn54 and Leu55, interact with the glycyl and cysteinyl moieties of GSH, respectively. An-

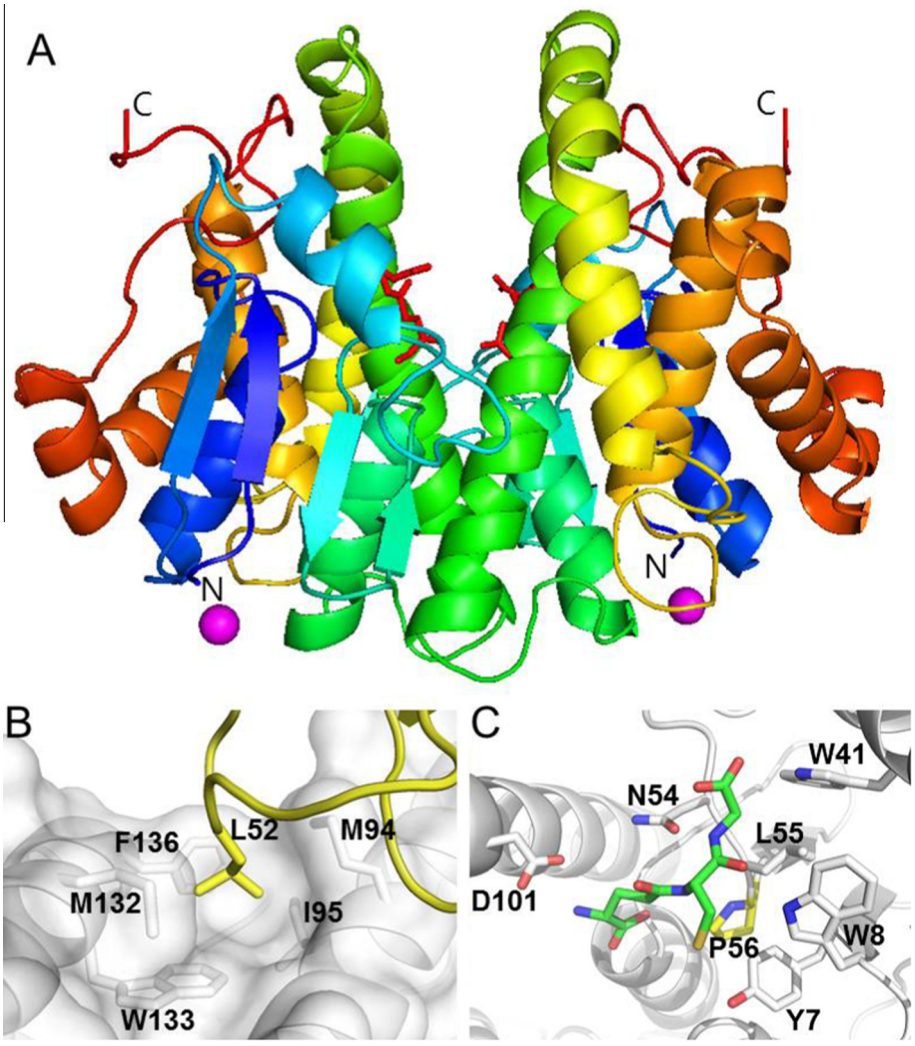

Fig. 1. The structural characteristics of *Cs*GST. (A) The two monomers of *Cs*GST form a dimer. Each monomer consists of two domains, the N-terminal and C-terminal domains. The two GSH substrates (red stick) bind to the N-terminus of each monomer. A zinc ion (magenta sphere) is coordinated in N-terminal domain. Each monomer is shown in rainbow color. The N- and C-terminal ends are represented as blue and red, respectively. (B) Hydrophobic interaction in the dimerization interface. The Met94, Ile95, Met132, Trp133 and Phe136 of the C-terminal domain of one monomer are clustered and form a concave hydrophobic pocket. Leu52 (yellow stick) of the N-terminal domain of the other monomer forms a hydrophobic interaction in a knob-and-hole manner. (C) The GSH binding site. The GSH (green stick) binds to each N-terminal domain. The N-terminal domain residues Tyr7, Trp8, Trp41, Asn54, Leu55, and Pro56 and Asp101 of the C-terminal domain of the other monomer interact with GSH. Notably, Pro56 (yellow) adapts a *cis* conformation that is characteristic of thioredoxin-like fold proteins. (For interpretation of the references to color in this figure legend, the reader is referred to the web version of this article.)

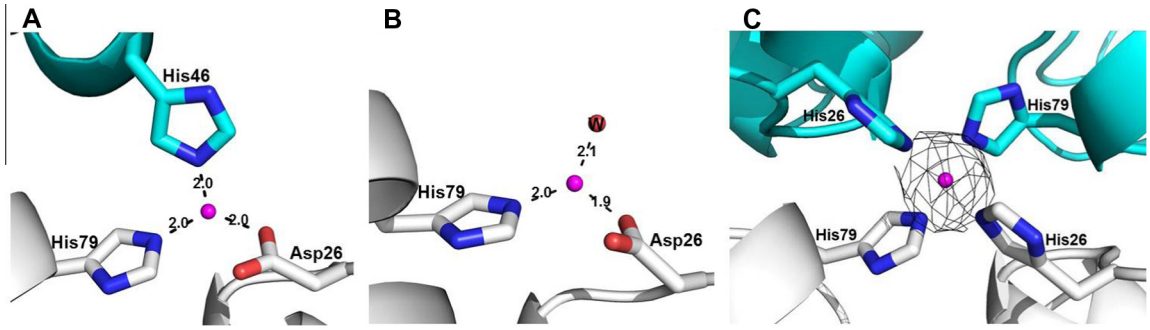

Fig. 2. The zinc ion coordination. (A) Asp26, His 79 (white) and His46 (cyan) of the adjacent molecule coordinate a zinc ion (magenta) in space group $P2_12_12_1$. The three residues are located 2.0 Å from the zinc ion. (B) Asp26, His79 (white) and a water molecule (red) coordinate a zinc ion in space group $P3_221$. (C) Four histidine residues coordinate a zinc ion. His79, substituted His26 of one monomer (white) and the two histidine residues of a neighbor molecule (cyan) form a tetrahedral arrangement 2.0 Å from the zinc ion (magenta). The electron density around the zinc ion is represented at 1σ. (For interpretation of the references to color in this figure legend, the reader is referred to the web version of this article.)

other characteristic of mu class GSTs is that the catalytic tyrosine residue in the N-terminal domain stabilizes the thiol group of GSH by a hydrogen bond [14]. The hydroxyl group of the Tyr7 side chain is located 3.2 Å away from the thiol group of GSH and forms a hydrogen bond. Two Trp residues, Trp8 and Trp41, are located close to Tyr7 and participate in the interaction through the η^2 nitrogen atom of the side chain with the cysteinyl carboxyl group and glycine of GSH, respectively. The carboxyl group of Asp101 of the opposite subunit forms a salt bridge with the amino group of the GSH γ-glutamyl (Fig. 1C).

3.2. Zinc coordination

Even though the two crystallization conditions of *Cs*GST are different in pH and precipitant, a small amount of zinc ion was included in the both solutions. The zinc ion is essential for the crystallization of *Cs*GST.

In the orthorhombic $P2_12_12_1$ crystal system, a zinc ion is coordinated by three residues, Asp26, His46 and His79. Asp26 and His79 are in one monomer of the homo-dimeric GST and the other, His46, comes from a neighbor molecule in crystal packing (Fig. 2A). All three residues are located 2.0 Å from the zinc atom. Asp26 Oδ1, His79 Nε2 and His46 Nε2 compose the triangular geometry of the zinc coordination (Fig. 2A). Each subunit of the dimer contains two zinc-binding regions – one is Asp26 and His79, and the other is His46. Each binding region contacts two different molecules through the zinc ion coordination (Fig. 3A). This results in the molecules being arranged in a 2_1 screw at three axes.

In the trigonal $P3_221$ crystal system, a zinc ion is coordinated by Asp26, His79 and a water molecule (Fig. 2B). Instead of the histidine residue from a symmetry-related molecule, the water molecule coordinates the zinc ion at 2.1 Å (Fig. 2B). The coordinated zinc ions do not influence the crystal packing (Fig. 3B).

The zinc ion is a divalent metal cation found abundantly in protein structures. Most zinc ions are coordinated by four residues, either all cysteines or three cysteines and one histidine as electron donors. In other cases, zinc is often coordinated by coordination number (CN) three, in which case the most frequent atoms are the N atom of imidazole, O atom of carboxyl and water. The mean distances between the zinc and coordinating atoms are 2.07 Å for the imidazole N atom, 2.11 Å for the carboxyl O atom, 2.33 Å for the cysteinyl S atom and 2.18 Å for water [29].

The zinc ion coordination in *Cs*GST adopts typical CN3 characteristics.

3.3. Mutation of Asp to His

*Cs*GST coordinates the zinc ion in two different combinations, His–Asp–His and His–Asp–water. Although particular amino acids – Cys, His, Glu and Asp – are incorporated in zinc coordination, there are three times more His involved than Asp [29]. To enhance the contribution of the more frequently utilized amino acid, *Cs*GST Asp26 was mutated to histidine. *Cs*GST–D26H was crystallized in the same conditions that yielded a native crystal in the space group $P3_221$, but the space group changed to $P3_121$ (Table 1). The packing

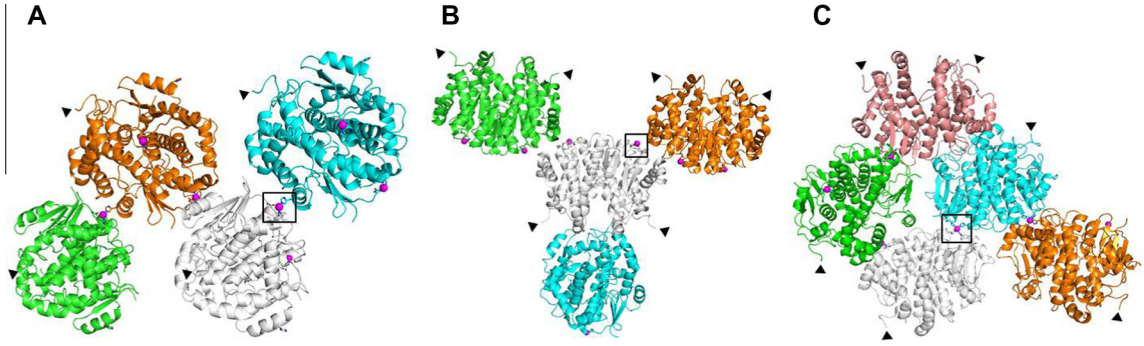

Fig. 3. The molecular arrangement in crystal packing. The three crystal structures contain different crystal systems – $P2_12_12_1$, $P3_221$ and $P3_121$. All protein molecules contact adjacent molecules due to crystal packing. In the $P2_12_12_1$ (A) and $P3_121$ (C) system, the zinc ions (magenta) contact neighbor molecules by coordination. However, the coordinated zinc ions do not participate in molecular contact in the $P3_221$ system (B). All C-terminal ends are exposed to solvent and indicated by an arrowhead. The zinc coordination regions represented in Fig. 2 are indicated as black squares. (For interpretation of the references to color in this figure legend, the reader is referred to the web version of this article.)

orientation of *Cs*GST–D26H against the trigonal screw axis in unit cell changed to the opposite direction to that of space group $P3_221$.

Except for the zinc coordination, the mutant structure is quite similar to the native one. Instead of the water molecule coordination seen in the native crystal, the substituted His26 and His79 of a neighbor molecule in crystal packing participate in the coordination of a zinc ion (Fig. 2C). The four histidineresidues coordinate a zinc ion in a tetrahedral arrangement. Tetrahedral geometry is found dominantly in examples of zinc coordination in protein structures due to the equilibrium between the attractive electrostatic metal–ligand forces and the repulsion of the bound residues [30]. The mutation of Asp26 to histidine changed the zinc coordination to the most frequent CN and geometry. One zinc ion connects two distinguishable dimers through coordination by subunits of each dimer in the molecular contact region (Fig. 3C).

4. Discussion

It appears that the zinc ion is necessary for the crystallization of native and mutant *Cs*GST. We could not generate good orthorhombic crystals of *Cs*GST or *Cs*GST–D26H in the absence of zinc ions. Interestingly, the zinc ions in the orthorhombic system and the D26H mutant are located at a molecular contact interface (Fig. 3A and C). The zinc coordination may induce a reduction in the distance between two molecules of *Cs*GST and facilitate the hand-in-hand arrangement of the molecules in a crystalline state. Although the zinc ions are not in the molecular contact region of the trigonal system (Fig. 3B), the crystal quality improved in the presence of zinc ions. Some ugly crystals of the trigonal system became suitable for diffraction after the addition of a small amount of zinc ion. When Glu26 of *Sj*GST, which corresponds to Asp26 of *Cs*GST, was mutated to histidine, the nickel ion-binding affinity increased [21]. These data suggested that the harmony of the His79 and the substituted His26 is a putative metal binding site.

Three types of crystals were formed in different crystal systems. Regardless of the crystal system, all the C-terminal ends are exposed to solvent (Fig. 3). These results reflect that *Cs*GST and *Cs*GST–D26H mutant crystals have enough solvent space to be useful in fused peptides. We therefore propose that *Cs*GST and *Cs*GST–D26H could be useful as crystallization carrier proteins in the presence of zinc ion.

Acknowledgments

This work was supported by a KBSI grant (T33410) to C.H.-K. and a research grant from Chungbuk National University in 2011. We thank the staff of beamline PAL-4A and PAL-6C at the Pohang Acceleratory Laboratory for their assistance with data collection.

References

[1] R.N. Armstrong, Structure, catalytic mechanism, and evolution of the glutathione transferases, Chem. Res. Toxicol. 10 (1997) 2–18.
[2] J.D. Hayes, D.J. Pulford, The glutathione S-transferase supergene family: regulation of GST and the contribution of the isoenzymes to cancer chemoprotection and drug resistance, Crit. Rev. Biochem. Mol. Biol. 30 (1995) 445–600.
[3] C. Frova, Glutathione transferases in the genomics era: new insights and perspectives, Biomol. Eng. 23 (2006) 149–169.
[4] D. Sheehan, G. Meade, V.M. Foley, C.A. Dowd, Structure, function and evolution of glutathione transferases: implications for classification of non-mammalian members of an ancient enzyme superfamily, Biochem. J. 360 (2001) 1–16.
[5] H. Dirr, P. Reinemer, R. Huber, X-ray crystal structures of cytosolic glutathione S-transferases. Implications for protein architecture, substrate recognition and catalytic function, Eur. J. Biochem. 220 (1994) 645–661.
[6] M.C. Wilce, M.W. Parker, Structure and function of glutathione S-transferases, Biochim. Biophys. Acta 1205 (1994) 1–18.
[7] K. Lim, J.X. Ho, K. Keeling, G.L. Gilliland, X. Ji, F. Rüker, D.C. Carter, Three-dimensional structure of *Schistosoma japonicum* glutathione S-transferase fused with a six-amino acid conserved neutralizing epitope of gp41 from HIV, Protein Sci. 3 (1994) 2233–2244.
[8] M.A. McTigue, D.R. Williams, J.A. Tainer, Crystal structures of a schistosomal drug and vaccine target: glutathione S-transferase from *Schistosoma japonica* and its complex with the leading antischistosomal drug praziquantel, J. Mol. Biol. 246 (1995) 21–27.
[9] J. Rossjohn, S.C. Feil, M.C. Wilce, J.L. Sexton, T.W. Spithill, M.W. Parker, Crystallization, structural determination and analysis of a novel parasite vaccine candidate: *Fasciola hepatica* glutathione S-transferase, J. Mol. Biol. 273 (1997) 857–872.
[10] K.A. Johnson, F. Angelucci, A. Bellelli, M. Hervé, J. Fontaine, D. Tsernoglou, A. Capron, F. Trottein, M. Brunori, Crystal structure of the 28 kDa glutathione S-transferase from *Schistosoma haematobium*, Biochemistry 42 (2003) 10084–10094.
[11] O.A. Asojo, K. Homma, M. Sedlacek, M. Ngamelue, G.N. Goud, B. Zhan, V. Deumic, O. Asojo, P.J. Hotez, X-ray structures of Na-GST-1 and Na-GST-2 two glutathione S-transferase from the human hookworm *Necator americanus*, BMC Struct. Biol. 7 (2007) 42.
[12] P.M. Brophy, J. Barrett, Glutathione transferase in helminths, Parasitology 100 (1990) 345–349.
[13] W.Y. Precious, J. Barrett, The possible absence of cytochrome P-450 linked xenobiotic metabolism in helminths, Biochim. Biophys. Acta 992 (1989) 215–222.
[14] A. Torres-Rivera, A. Landa, Glutathione transferases from parasites: a biochemical view, Acta Trop. 105 (2008) 99–112.
[15] J.L. Sexton, A.R. Milner, M. Panaccio, J. Waddington, G. Wijffels, D. Chandler, C. Thompson, L. Wilson, T.W. Spithill, G.F. Mitchell, N.J. Campbell, Glutathione S-transferase. Novel vaccine against *Fasciola hepatica* infection in sheep, J. Immunol. 145 (1990) 3905–3910.
[16] I. Ferru, B. Georges, M. Bossus, J. Estaquier, M. Delacre, D.A. Harn, A. Tartar, A. Capron, H. Grassmasse, C. Auriault, Analysis of the immune response elicited by a multiple antigen peptide (MAP) composed of two distinct protective antigens derived from the parasite *Schistosoma mansoni*, Parasite Immunol. 19 (1997) 1–11.
[17] S.C. Jao, J. Chen, K. Yang, W.S. Li, Design of potent inhibitors for *Schistosoma japonica* glutathione S-transferase, Bioorg. Med. Chem. 14 (2006) 304–318.
[18] D.B. Smith, K.S. Johnson, Single-step purification of polypeptides expressed in *Escherichia coli* as fusions with glutathione S-transferase, Genetics 67 (1988) 31–40.
[19] G. Chaga, M. Widersten, L. Andersson, J. Porath, U.H. Danielson, B. Mannervik, Engineering of a metal coordinating site into human glutathione transferase M1-1 based on immobilized metal ion affinity chromatography of homologous rat enzymes, Protein Eng. 7 (1994) 1115–1119.
[20] S. Yilmaz, M. Widersten, T. Emahazion, B. Mannervik, Generation of a Ni(II) binding site by introduction of a histidine cluster in the structure of human glutathione transferase A1-1, Protein Eng. 8 (1995) 1163–1169.
[21] Y.H. Han, H.A. Seo, G.H. Kim, C.K. Lee, Y.K. Kang, K.H. Ryu, Y.J. Chung, A histidine substitution confers metal binding affinity to a *Schistosoma japonicum* glutathione S-transferase, Protein Expr. Purif. 73 (2010) 74–77.
[22] Y.H. Han, Y.H. Chung, T.Y. Kim, S.J. Hong, J.D. Choi, Y.J. Chung, Crystallization of *Clonorchis sinensis* 26 kDa glutathione S-transferase and its fusion proteins with peptides of different lengths, Acta Crystallogr., Sect. D: Biol. Crystallogr. 57 (2001) 579–581.
[23] Z. Otwinowski, W. Minor, Processing of X-ray diffraction data collected in oscillation mode, Methods Enzymol. 276 (1997) 307–326.
[24] T.G. Battye, L. Kontogiannis, O. Johnson, H.R. Powell, A.G. Leslie, IMOSFLM: a new graphical interface for diffraction-image processing with MOSFLM, Acta Crystallogr., Sect. D: Biol. Crystallogr. 67 (2011) 271–281.
[25] A. Vagin, A. Teplyakov, MOLREP: an automated program for molecular replacement, J. Appl. Crystallogr. 30 (1997) 1022–1025.
[26] P. Emsley, B. Lohkamp, W.G. Scott, K. Cowtan, Features and development of Coot, Acta Crystallogr., Sect. D: Biol. Crystallogr. 66 (2010) 486–501.
[27] G.N. Murshudov, P. Skubák, A.A. Lebedev, N.S. Pannu, R.A. Steiner, R.A. Nicholls, M.D. Winn, F. Longa, A.A. Vagina, REFMAC5 for the refinement of macromolecular crystal structures, Acta Crystallogr., Sect. D: Biol. Crystallogr. 67 (2011) 355–367.
[28] C. Nathaniel, L.A. Wallace, J. Burke, H.W. Dirr, The role of an evolutionarily conserved *cis*-proline in the thioredoxin-like domain of human class Alpha glutathione transferase A1-1, Biochem. J. 372 (2003) 241–246.
[29] I. Dokmanic, M. Sikic, S. Tomic, Metals in proteins: correlation between the metal–ion type, coordination number and the amino-acid residues involved in the coordination, Acta Crystallogr., Sect. D: Biol. Crystallogr. 64 (2008) 257–263.
[30] L. Rulísek, J. Vondrásek, Coordination geometries of selected transition metal ions (Co^{2+}, Ni^{2+}, Cu^{2+}, Zn^{2+}, Cd^{2+}, and Hg^{2+}) in metalloproteins, J. Inorg. Biochem. 71 (1998) 115–127.